ATAD2 drives HIRA/histone H3.3-dependent chromatin dynamics

Ariadni Liakopoulou[1], Fayçal Boussouar[1#], Daniel Perazza[1], Sophie Barral[1], Emeline Lambert[1], Tao Wang[1], Florent Chuffart[1], Ekaterina Bourova-Flin[1], Charlyne Gard[2], Denis Puthier[2], Sophie Rousseaux[1], Christophe Arnoult[1], André Verdel[1], Saadi Khochbin[1#]

1- Univ. Grenoble Alpes, CNRS UMR 5309 and INSERM U1209, Institute for Advanced Biosciences, 38706, La Tronche, France

2- Aix Marseille Université, INSERM, TAGC, TGML, 13288, Marseille, France

correspondence:

Saadi Khochbin: saadi.khochbin@univ-grenoble-alpes.fr

Fayçal Boussouar: faycal.boussouar@univ-grenoble-alpes.fr

Abstract

ATAD2, expressed predominantly in embryonic stem cells as well as in spermatogenic cells emerges as a pivotal regulator of chromatin dynamics by mediating chromatin-bound histone chaperone turnover. Here, investigating the role of ATAD2 in spermatogenesis, we show that through its preponderant expression in haploid male germ cells, ATAD2 modulates the HIRA-dependent H3.3 genome localization and H3.3-dependent gene transcriptional regulation. Furthermore, by influencing histone eviction and the assembly of protamines, it ensures proper chromatin condensation and genome packaging in mature spermatozoa. The disruption of *Atad2* results in aberrant mature spermatozoa genome organization, impacting male fertility. Collectively, these findings confirm the occurrence of an overlooked chromatin dynamic regulatory level controlling histone deposition-removal balance, depending on an ATAD2-controlled histone chaperone – chromatin interaction.

Introduction

Spermatogenesis involves unique and dramatic chromatin remodelling and genome reorganization events that take place in preparation of a shift from the universal nucleosome-based eukaryotic genome organization into a unique nucleoprotamine-based structure (Gaucher et al. 2010; Bao and Bedford 2016; Le Blevec et al. 2020; Okada 2022). During the last decade, important information on the molecular basis of the nucleosome-to-nucleoprotamine transition became available. Several testis-specific H2A, H2B and H3 histone variants locally or globally replace the canonical histones at different stages, starting early during the commitment of cells into meiotic and post-meiotic differentiation (Hoghoughi et al. 2018). Most of this nucleosome dismantlement and assembly occurs in the absence of DNA replication. In other words, the replication-independent nucleosome assembly pathways, such as the well-documented HIRA-dependent H3.3 assembly, are expected to be critical in ensuring the necessary chromatin dynamics in these cells. Finally, hints on the functions of transition proteins (TPs), and their functional relationship with protamines (PRMs) were proposed based on the study of a specific late-expressing H2A variant, H2A.L.2 (Barral et al. 2017b). Basically, it has been suggested that TPs do not directly replace histones, but could be loaded on open H2A.L.2-containing nucleosomes to control PRM assembly. Nucleosome-to-nucleoprotamine transition also includes a TP-dependent prePRM2 processing, histone displacement by PRMs and the structuration of the nucleoprotamine-based genome organization in the mature spermatozoa (Barral et al. 2017b; Rezaei-Gazik et al. 2022).

Taking into account this unique dynamic of post-meiotic cells' nucleosomes, it is expected that these cells massively express generic or germline-specific factors acting on chromatin including histone acetylating machineries, acetylated histone readers and histone variants and their chaperones mediating these histone and non-histone protein exchanges. Most specifically, the replication-independent nature of nucleosome assembly, both in cells undergoing meiosis and in post-meiotic cells, strongly suggests the involvement of the chaperone / histone substrate couple, HIRA and H3.3.

An important part of this replication-independent histone assembly and transitions in the genome organizations occurs in the context of a massive histone H4 hyperacetylation in the haploid spermatogenic cells, spermatids, mediated by NUT-p300/CBP histone acetyltransferase complex (Shiota et al. 2018; Rousseaux et al. 2022). Hyperacetylation of histone H4, specially, the double acetylation on H4K5K8 in these cells, leads to the binding of

H4 by the first bromodomain of BRDT and histone replacement (Moriniere et al. 2009; Gaucher et al. 2012; Goudarzi et al. 2016; Shiota et al. 2018). Additionally, Histone H4 hyperacetylation, specially at H4K5, could also be recognized by another bromodomain-containing factor of unknown function in spermatogenic cells, ATAD2 (Caron et al. 2010; Morozumi et al. 2016).

ATAD2 is a conserved bromodomain-containing factor harbouring in addition, an AAA ATPase domain (Boussouar et al. 2013; Cattaneo et al. 2014). Our early work showed that *Atad2* is predominantly expressed in embryonic stem cells (ES cells), as well as in spermatogenic cells, and is aberrantly activated in virtually all solid cancers (Caron et al. 2010). Although ATAD2's function in cancer prompted many investigations (Liu et al. 2022), its function in its physiological context of expression remained largely overlooked. We reported the first investigations of ATAD2's function in embryonic stem cells (Morozumi et al. 2016). These studies in ES cells showed that ATAD2 is recruited into acetylated transcriptionally active chromatin and is critical to keep the chromatin of ES cells highly dynamic, as illustrated by an ATAD2-dependent high rate of histone exchange (Morozumi et al. 2016). Later studies by our laboratory deciphered the molecular basis of this activity of ATAD2, which relies on its capacity to ensure the turnover of chromatin-bound histone chaperone, HIRA, in both yeast *S. pombe* and in mouse ES cells (Wang et al. 2021). In addition to ES cells, *Atad2* is also highly expressed in male germ cells, pointing to its potential role in the regulation of HIRA -dependent H3.3 assembly in these cells, specially, in post-meiotic cells. Indeed, previous published works have highlighted the important function of H3.3 assembly in meiotic and post-meiotic male genome programming (van der Heijden et al. 2007; Yuen et al. 2014; Tang et al. 2015; Fontaine et al. 2022). We therefore hypothesized that the ATAD2-controlled HIRA-H3.3 activity would also be a critical player in post-meiotic male genome reorganization, as HIRA has been shown to be essential post-fertilization (Lin et al. 2014) and during oogenesis (Nashun et al. 2015).

Using a *Atad2* KO mouse model, we could show that *Atad2*'s expression is dramatically enhanced in post-meiotic male germ cells, ensuring a proper dynamics of histone H3.3, including on the sex chromosomes. More remarkably, our data demonstrate that ATAD2 controls the appropriate expression of a series of genes whose activity is known to be H3.3-dependent in post-meiotic cells. Additionally, in the absence of ATAD2, perturbed nucleosome dynamics leads to a delayed histone-to-PRM-replacement, leading to a defective global final male genome compaction. Although this defective mature spermatozoon genome

compaction has little effect on male fertility following natural reproduction, it severely impacts the success of *in vitro* fertilization using spermatozoa from *Atad2* KO mice.

In summary, our work identified a yet unknown level of the regulation of chromatin plasticity, involving the control of histone chaperone dynamics, particularly that of HIRA, controlling the proper male transcriptional regulation, genome compaction and optimal male fertility.

Results

Atad2 is predominantly expressed in haploid male germ cells

Atad2 is normally expressed in ES and spermatogenic cells and remains silent in the majority of adult tissues (Morozumi et al. 2016). Therefore, in addition to ES cells, male germ cells constitute the second cell type where the molecular basis of the physiological ATAD2 activity could be investigated.

To decipher the function of ATAD2 during spermatogenesis, we have first considered the stage-specific expression of *Atad2*. This task was facilitated by the utilization of a mouse model which allows for a *Cre/LoxP*-dependent deletion of *Atad2's* exon 12. In addition, insertion of a *lacZ* reporter cassette enables fusion of the *lacZ* transgene with exon 11 of *Atad2* and production of a non-functional ATAD2-lacZ fusion protein (Fig. 1A). In the mouse testis, *Atad2* gives rise to two protein variants, a long form, ATAD2L and a short testis-specific form, that we previously named ATAD2S (Caron et al. 2010). The combined LacZ fusion and *Cre recombinase*-dependent deletion of *Atad2's* exon 12 leads to the disappearance of both ATAD2L and ATADS (Fig. 1B).

The expression of *lacZ* under the *Atad2* promoter allows one to visualize *Atad2* gene activity in a stage-specific manner. X-gal staining of seminiferous tubule sections from *Atad2* KO mice showed a remarkably high expression of *Atad2* in post-meiotic spermatogenic cells (Fig. 1C). No staining was observed in the wild-type tubules.

ATAD2 controls HIRA accumulation

In our previous work performed in parallel in *S. pombe* and in mouse ES cells, we could demonstrate a critical role for ATAD2 in HIRA-dependent histone dosage as well as in HIRA-chromatin interaction in both yeast and mouse ES cells. Among other discoveries, this work showed that in the absence of ATAD2, HIRA becomes trapped on chromatin leading to its

accumulation in ES cells, as well as in a variety of cancers cells (Wang et al. 2021). Because of this very conserved action of ATAD2 in controlling the HIRA activity, we reasoned that the ATAD2-dependent HIRA activity should be particularly active during the spermatogenic cell differentiation, specially, in post-meiotic spermatogenic cells, when ATAD2 expression is highly induced (Fig. 1C). To test if the absence of ATAD2 could lead to the accumulation of HIRA as we previously reported in other systems, we quantified HIRA in spermatogenic cells from both wild-type and *Atad2* KO mice. These investigations revealed an accumulation of HIRA in *Atad2* KO spermatogenic cells (Fig. 2A), consistent with its increased association with chromatin (Wang et al. 2021). We have also monitored HIRA accumulation as a function of spermatogenic cells stages. Because of the dramatic activation of *Atad2* after meiosis, in round spermatids, the ATAD2-dependent accumulation of HIRA was expected to mostly occur in round spermatids. Accordingly, we also compared HIRA accumulation in fractionated spermatogenic cell extracts. Figure 2B shows that in agreement with the action of ATAD2, particularly on the post meiotic cells' chromatin, we can observe that when ATAD2 is absent, the accumulation of HIRA mostly occurs in round spermatids.

ATAD2 controls HIRA-dependent H3.3 localization and H3.3-dependent transcription

An increased presence of HIRA on chromatin in the absence of ATAD2, should also be associated with increased amounts of deposited histones, as demonstrated previously, specially, in *S. pombe*, since histone gene inactivation could rescue the absence of *Atad2*/*Abo1* and in ES cells, where an increased nucleosome assembly occurs, even on the so-called nucleosome-free region (NFR) (Wang et al. 2021).

Interestingly, visualization of H3.3, the major target of HIRA by immunofluorescence in round spermatids, showed an increased labelling of H3.3 (Fig. 3), which is known to normally concentrate on the sex chromosomes (van der Heijden et al. 2007; Fontaine et al. 2022). Indeed, as expected and previously reported, in the wild-type round spermatids, H3.3 was mostly observed in a single domain, close to the unique chromocenter in these cells (Fig. 3, left panels). In the absence of ATAD2, in agreement with an increased residence time of HIRA on chromatin in general and a reduced H3.3 turnover, an increased level of H3.3 could be observed on the sex chromosome (adjacent to the chromocenter), and more interestingly, on all over the genome (Fig. 3, right panels).

In order to definitively confirm our working hypothesis on the ATAD2-HIRA-H3.3 functional interaction, we took advantage of published H3.3-dependent transcriptomic data (Fontaine et al. 2022). Indeed, the authors of this publication identified a series of genes that are mis-regulated in cells with inactivated *H3.3b* gene. Because of the post-meiotic major activation of *Atad2*, we specifically focussed on the gene lists that show a H3.3-dependent deregulated expression in post-meiotic round spermatid.

To this end, we followed whole genome transcriptional activity during the first wave of spermatogenesis at day 20 post-partum (PP), when meiosis is complete and when the first post-meiotic cells accumulate on 22-, 24- and 26-days PP.

In these transcriptomes, we specifically followed the expression of the published lists of genes that are downregulated or upregulated in the absence of H3.3 (Fontaine et al. 2022). Very interestingly, we observed that the majority of genes that were reported to be down regulated in the absence of H3.3 (meaning they require H3.3 to be active; H3.3-activated genes), are upregulated in the absence of ATAD2, particularly at day 26 PP, when a significant number of post-meiotic cells accumulate (Fig. 4A). This phenomenon could also be observed when genes that were up-regulated in the absence of H3.3 were considered (meaning genes that are repressed by H3.3). In this case, the absence of ATAD2 led to the enhancement of their down-regulation. In other words, the absence of ATAD2 led to an enhancement of H3.3-dependent gene repression (Fig. S1).

Fontaine and colleagues also reported that sex chromosome-linked genes that normally undergo meiotic sex chromosome transcriptional inactivation, were up-regulated in the absence of H3.3, meaning that H3.3 is required for their repression. We also considered these genes and showed that they present an enhancement of repression in the absence of ATAD2 (Fig. 4B).

These analyses clearly indicate that the absence of ATAD2 enhances H3.3 functions in agreement with increased residence time of H3.3 in nucleosomes. Genes that require H3.3 to be repressed or activated present an enhanced repression or activation respectively in the absence of ATAD2.

Overall, these investigations remarkably confirmed a role for ATAD2 in regulating H3.3 function.

ATAD2 is required for controlled histone eviction and PRM assembly

Taking into account ATAD2's role in HIRA - chromatin interaction dynamics and hence that of H3.3 assembly in post-meiotic cells, as well as ATAD2's similar role in the dynamics of other histone chaperones such as FACT (Wang et al. 2021), ATAD2 could be considered also as a good candidate in controlling the histone-to-protamine replacement, which occurs later in these cells. The histone eviction process involves a genome-wide histone H4 hyperacetylation (Shiota et al. 2018) and a TP-mediated PRMs assembly, which directs histone eviction and the final packing of the male genome (Barral et al. 2017a). To test the involvement of ATAD2 in spermatogenic cell chromatin reorganization, we sought to co-detect testis-specific H2B variant, TH2B (Montellier et al. 2013), along with transition protein 1 (TP1) and protamine 1 (PRM1). TH2B is first expressed at the commitment of spermatogenic cells into meiotic divisions and progressively becomes the major H2B species of spermatogenic cell chromatin in the subsequent stages (Montellier et al. 2013). As expected, the accumulation of TP1 and Prm1 in wild-type cells is associated with the eviction of the majority of histones, reflected by the mutually exclusive labelling of TH2B and TP1/Prm1 in distinct cells (Fig. 5A and 5B, wild-type mice). In contrast, in *Atad2* KO cells, TH2B and TP1/Prm1 were co-detected in a significant number of cells (Fig. 5A and 5B), suggesting that the process of histone eviction is disturbed. However, in the *Atad2* KO cells, the observed impairment of histone removal is transient since spermatids with dominating amounts of TP1 and Prm1 eventually appear (Fig. 5).

These observations strongly suggest that, in the absence of ATAD2, the process of histone eviction is also slowed down, allowing for the simultaneous detection of histones and histone-replacing proteins in the same cells.

Since the NUT-CBP/p300 - dependent H4 hyperacetylation, as well as the expression of H2A.L.2, TPs and PRMs are also required for histone removal, we also tested if the observed delay in histone removal is not due to a defective histone acetylation, specially at H4K5, as well as a perturbed cell type-specific expression and localization of H2A.L.2, TPs and PRMs. Immunohistochemistry detection of H4K5ac, TP2, PRM1, PRM2 did not detect any remarkable change in H4K5 acetylation levels or the expression and cell type-specificity of the investigated proteins (Fig. S2).

These data support the idea that the perturbed modified dynamics of histone/TP/PRM chaperones does not grossly affect the other molecular events involved in the histone-to-PRM replacement.

Perturbed pre-PRM2 processing in the absence of ATAD2

Previously, we could show that the incorporation of TPs on nucleosome (a H2A.L.2-dependent process) is required for the proper processing of pre-PRM2. In the absence of ATAD2, the abnormal overlapping histone, TP and protamine co-detection, suggested that TPs would not properly mediate the pre-PRM processing. To test this prediction, we took advantage of our specific pre-PRM2 antibody (Rezaei-Gazik et al. 2022) to visualize in the cells the presence of pre-PRM2 undergoing the process of maturation and assembly. Figure 6 shows that although pre-PRM2 is present in both wild-type and *Atad2* KO elongating spermatids, in the absence of ATAD2, pre-PRM2 tends to form dense aggregates as well as fragmented genomic domains. This phenomenon is also associated with an increased accumulation of pre-PRM2 in testis extracts of *Atad2* KO spermatogenic cells (Fig. 6B).

These data strongly support the idea that ATAD2 is required to streamline the activity of histone chaperones as well as of factors involved in histone exchange and TP/PRM assembly.

Defective mature spermatozoa genome organization and male fertility

The *Atad2* KO post-meiotic cells' defective chromatin organization although not affecting the testis histology (data not shown), impacts testis weight and sperm count, which are significantly reduced in *Atad2* KO mice (Fig. S3).

As expected, the impact of ATAD2 on HIRA function and TP/PRM assembly has also an impact on propre sperm genome compaction. Indeed, mature sperm genome decompaction test revealed a significant difference in ability of the genome to resist genome decompacting conditions between the spermatozoa of wild-type and *Atad2* KO mice (Fig. 7A). Since poor quality spermatozoa with detective genome compaction are known to poorly support *in vitro* fertilization (Bashiri et al. 2021), we expected that spermatozoa from *Atad2* KO mice would do poorly in *in vitro* fertilization assays compared to the wild-type spermatozoa. Figure 7B shows that this is indeed the case. However, surprisingly, fertility tests carried out on sexually mature adult males revealed that *Atad2* KO male mice are fertile, with only a statistically non-

significant effect observed on their ability to foster pups (Fig. 7C), indicating that *in vivo* fertilization could buffer a relatively large series of sperm genome compaction defaults.

Discussion

Previously, taking advantage of the very conserved structural features of ATAD2 and relying on the power of yeast genetics, we discovered that ATAD2's function is mostly to control major histone chaperone functions. Using a screen of the Abo1/ATAD2-dependent arrest of *S. pombe* cell growth, we found that impressively, 11 of the 14 suppressor mutations (growth arrest suppression) impacted histone chaperones or histones themselves, with 8 distinct inactivating mutations in the histone chaperone HIRA complex. Investigation of mouse ES cells showed that in the absence of ATAD2, HIRA accumulates and remains bound to nucleosomes, leading to nucleosome overloading around active gene transcriptional start sites (TSSs) and on the normally nucleosome-free regions (NFRs) of these genes.

Here, we showed that *Atad2* is highly activated in post-meiotic spermatogenic cells and that in its absence, as in ES cells and in different cancer cells, HIRA accumulates. Our new data suggest that in the absence of ATAD2 activity, HIRA residency time on chromatin increases leading to decreased dynamics and overloading of its substrate, histone H3.3. This replication-independent histone has been first shown to assemble on the transcriptionally inactive meiotic cell sex chromosomes by Peter de Boer's laboratory (van der Heijden et al. 2007). Subsequent studies showed that H3.3 remained enriched on the sex chromosomes also in early post-meiotic cells, usually localized close to the unique large chromocenter in these cells (Fontaine et al. 2022).

In agreement with a role for ATAD2 in the control of HIRA-dependent dynamics of H3.3, we observed a more intense labelling of H3.3 on the sex bodies in round spermatids and impressively, an increase in the genomic background detection of H3.3 in these cells.

The role of ATAD2 in the HIRA/H3.3 functions is also beautifully confirmed when the reported H3.3-depndent transcriptome was compared with the ATAD2-dependent transcriptome obtained here.

Indeed, in the absence of ATAD2, we observed an enhancement of H3.3-dependent gene regulatory events (activation or repression), in agreement with an increased H3.3 presence and hence function, in the chromatin of *Atad2* KO post-meiotic cells.

These investigations on ATAD2's function in post-meiotic spermatogenic cells extend our previous work in *S. pombe* and ES cells, and point to a yet overlooked level of regulation of histone dynamics, depending on the dynamics of histone chaperone - chromatin interaction. Previously, A. Groth's laboratory discovered that histone chaperone DNAJC9 recruits the ATPase HSP70 to provide the necessary energy to release the chaperone from chromatin (Hammond et al. 2021). Considering our data on the role of ATPase ATAD2 with respect to HIRA and that of ATPase HSP70 with respect to DNAJC9, we can propose that ATP energy is required for the proper function of histone chaperones in controlling histone turnover.

Interestingly, very recently, while this manuscript was in preparation, a pre-print article (Jang et al. 2024), demonstrated that the *S. pombe* Abo1/ATAD2, is required for ATP-dependent dissociation of the histone chaperone FACT from chromatin, particularly at transcription start sites (TSSs). In line with this conclusion, using ChIP-seq mapping of FACT in ES cells, in the absence of ATAD2, we were also able to observe an accumulation of nucleosome-bound FACT at the TSSs of active genes (Wang et al. 2021), supporting the idea that ATAD2 not only controls the dynamics of histone-bound HIRA but also that of other histone chaperones such as FACT.

In addition to histones dynamics, many chromatin-bound regulatory factors also need to dynamically interact with chromatin and hence ATAD2 could also be involved in mediating the dynamic interactions of various chromatin-bound factors. In agreement with this hypothesis, our previously published proteomic studies of ATAD2-bound nucleosomes in ES cells highlighted the co-purification of various chromatin bound factors (Morozumi et al. 2016). Other AAA ATPase factors such as p97/VCP, have also demonstrated actions in the dynamics of chromatin-bound factors. Indeed, the AAA ATPase factor, p97/VCP, has been shown to remove H3 variant CENP-A (van den Berg et al. 2023), the chromatin trapped PARP1 (Krastev et al. 2022), trapped Ku70/80 (van den Boom et al. 2016), DNA damage sensors, DDB2 and XPC (Puumalainen et al. 2014), RNA polII (Lafon et al. 2015), and other chromatin interacting factors. Similarly, ATAD2 AAA ATPase very likely acts on other chromatin-bound factors than histone chaperones. However, due to its bromodomain, in contrast to p97/VCP, ATAD2 would preferentially act on H4K5 acetylated chromatin regions and would specifically ensure the dynamics of H4 acetylated chromatin-bound factors. Based on the data presented here, we can also include, a role for ATAD2 to streamline steps involving the H2A.L.2-dependent recruitment of TPs and protamine assembly and the final histone displacement in spermatids.

The chaperones involved in the TP/PRM assembly are not known, but it is possible that ATAD2 is also involved in the dissociation of these chaperones from their substrate proteins after their assembly. That is why in our *Atad2* KO spermatids, we observed an overlap between TP/PRM and histones. This could be due to the delayed removal of chaperones bound to TPs and PRMs and the inability of PrePRM2 to be processed and hence of PRMs to efficiently replace histones. Since histone replacement finally occurs in the absence of ATAD2, we can assume that other AAA ATPases such as p97/VCP, could come to rescue. However, under these conditions, although most of the histone replacement takes place, our functional tests such as *in vitro* chromatin decompaction and *in vitro* fertilization, strongly suggest that mature spermatozoa genome organization is not fully complete and the spermatozoa nuclei remain fragile and sensitive to external assaults.

In summary, the functional investigation of ATAD2 in the context of its physiological expression, during post-meiotic phases of spermatogenesis, confirmed our conclusion on the function of ATAD2 in ES cells as well as on its conserved activity of *S. pombe*. Collectively these investigations highlight a new level of the regulation of histone turnover and chromatin dynamics based on the control of histone-bound histone chaperone release.

Materials and Methods

Animal care and breading

Mice were housed at the Grenoble High Technology Animal Facility (PHTA). Mice were euthanized following a procedure approved by the official ethic committee of the University Grenoble Alpes (COMETH, C2EA-12). The investigators directly involved in care and breading of mice had an official animal-handling authorization obtained after 2 weeks of intensive training and a final formal evaluation.

Generation of *Atad2*-KO mice

Atad2 KO mice were obtained from the International Knockout Mouse Consortium, the Welcome Trust Sanger Institute, UK. The 'knockout-first' allele (tm1a) contains an IRES: *lacZ* trapping cassette and a floxed human β-actin promoter-driven *neo* cassette inserted into the intron 12 of the *Atad2* gene (Skarnes et al. 2011). We created *Atad2*$^{\Delta\ Neo\text{-}Exon\ 12}$ mice by crossing mice bearing the *tm1a* allele with CMV-Cre recombinase expressing mice. Subsequent Cre

expression under the control of a human cytomegalovirus (*CMV*) promoter results in an *Atad2*$^{LacZ\Delta Neo\text{-}Exon12}$ knockout mouse with the first 11 exons of Atad2 being fused to β-gal leading to a non-functional Atad2 protein depleted of its bromodomain and AAA ATPase domain.

Multiplex PCR genotyping for *Atad2*^{LacZ} was used to detect LacZ cassette producing a 393-bp WT band and a 293-bp mutant band using primers Atad2_84231_F, TATCCAACAAGCCTGAGCCC, Atad2_84231_R, CAACTGGAGCTGGGTCTTCC and Cas-R, TCGTGGTATCGTTATGCGCC.

Fertility test

Fertility tests were carried out with sexually mature 3-month-old males. Five WT males and five *Atad2* KO males were crossed with two C57BL6 females each during 3 months and the litter sizes were monitored during this period.

***In vitro* Fertilization**

Eggs were obtained from 6- to 7-week-old superovulated C57/BL6J females, stimulated by a first injection of 7.5 UI of PMSG (Pregnant Mare Serum Gonadotropin), followed 48 hours later by a second injection of 7.5 UI of HCG (Human Chorionic Gonadotropin). Fourteen hours later, females were euthanized by cervical dislocation and cumulus-oocytes complexes (COCs) released from the ampulla were collected in 500 µL M2 medium. Spermatozoa from wild type and *Atad2* KO males were harvested by dilaceration of the cauda epididymitis and allowed to swim in 1 mL M2 medium for 10 min at 37°C. Two hundred microliters of sperm were transferred into 800 µL M16 /2% BSA and capacitated for 80 min at 37°C /5% CO_2. Finally, 300,000 sperm were simultaneously added to the COCs and incubated in M16 medium at 37°C /5% CO_2. After 4 hours of incubation, unbound spermatozoa were removed by 3 successive washes with 500 µL of M16. Twenty-four hours after fertilization, unfertilized eggs and two-cell embryos (as an indication of successful fertilization), were scored.

Protein extraction and Immunoblotting

Proteins were extracted in Urea 8M, sonicated for 150J with a probe sonicator, mixed with 4x Laemli loading buffer and heated for 5 minutes at 95 °C. Protein samples were loaded on 4-

12% Bis-Tris gels and migrated at 150 V for 1h30. The transfer step was realized using a nitrocellulose membrane with the Bio-Rad Transfer Turbo machine. Nitrocellulose membrane was blocked in 5% milk PBS-Tween 0.1% solution, washed 3 times for 10 minutes with PBS-Tween 0.1% solution and incubated overnight at 4°C with specific antibodies listed in Table S1. Membranes were washed 3 times for 10 minutes with PBS-Tween 0.1% solution and were incubated with HRP secondary antibodies at 1/10000 dilution for 1h at RT under agitation. Revelation was performed using ECL substrates and visualization was performed with the Vilber Fusion FX Chemiluminescence imaging system (Vilber).

ELISA

Urea protein extracts were diluted in PBS and used to coat 96-well round bottom plates by incubating at 4°C overnight. Coating solution was removed and wells were washed 3 times with washing buffer (BSA 1%, PBS-T 0,1%). Wells were blocked with blocking buffer (5% BSA in PBS-T 0,1%) for 2 hours at room temperature under agitation. Blocking buffer was removed and wells were washed 2 times with washing buffer. Primary antibodies for PrePRM2 1:1000 and tubulin 1:5000 were diluted into blocking buffer, pipetted into their corresponding wells and incubated overnight at 4°C under mild agitation. Wells were washed 4 times with washing buffer and subsequent incubation with secondary HRP antibodies, diluted 1:5000 in blocking buffer, was performed for 1 hour at room temperature under mild agitation. Wells were washed 4 times with washing buffer, and TMB ELISA Substrate was added to wells and incubated until the color developed, at which time Stop Solution was added to the wells to stop the reaction. The signal was quantified using a plate reader at 450nm.

X-Gal staining

Male mice were euthanized by cervical dislocation. Testes were dissected out, drilled in 3 points and incubated overnight at 4°C under agitation in fixative solution (0.5% glutaraldehyde, 2 mM $MgCl_2$ and 5 mM EGTA in PBS). After incubation until equilibration in an equilibration buffer (30% sucrose, 2 mM $MgCl_2$ and 5mM EGTA in PBS), testes were frozen individually in OCT on dry ice. Frozen blocks were sectioned at 10 µm slices on Superfrost™ slides and let dry overnight. Slides were fixed with fixation buffer (0.2% glutaraldehyde, 100 mM $MgCl_2$ and 5 mM EGTA in PBS) for 10 min, washed with washing buffer (PBS, 0.02% NP-40, 0.01% Sodium deoxycholate and 2 mM $MgCl_2$) for 5min and incubated three times in 50% Ethanol for 5 min

each. Then the slides were stained with staining solution (2 mM $MgCl_2$, 0.02% NP-40, 0.01%Na Doc, 5 mM potassium ferricyanide, 10 mM potassium ferrocyanide and 0.5 mg/ml X-gal) in a wet chamber for several hours at 37℃. The slides were then washed with washing buffer for 5 min and with distilled water, and a counterstaining was performed with hematoxylin. Finally, the slides were washed with running tap water for several minutes and mounted with Dako fluorescent mounting medium.

Immunofluorescence staining of germ cells

Staged seminiferous tubules were prepared as detaled in Gaucher et al. 2012. In order to permeabilize the cells, the slides were then placed in 0.5% saponine, 0.2% Triton X-100, and 1 × PBS at RT for 15 min and washed for 5 min with PBS. The preparations were then incubated in 5% milk, 0.2% PBS-Tween blocking buffer, at RT for 30 min under agitation. The primary antibodies were diluted in 1% dry milk, 0.2% PBS-Tween buffer. The slides were incubated overnight with this diluted solution of the primary antibodies in a humidified chamber at 4℃ and then washed three times for 5 min each in the antibodies' dilution buffer. The secondary antibodies were diluted at 1:500 in the same buffer and incubated in a humidified chamber for 30 min at 37℃, and then washed as for the primary antibodies. The DNA was counterstained by Hoechst, and the slides were mounted using Dako fluorescent mounting medium.

Sperm decompaction test

Spermatozoa from wild type and *Atad2* KO males were harvested by dilaceration of the cauda epididymis and allowed to swim in 1 mL M2 medium for 10 min at 37°C. The sperm-containing suspension was transferred into a 1.5 ml tube and centrifuged at 3000 rpm for 8 min in 4℃. The sperm pellets were resuspended in PBS and dropped onto glass slides to spread and dry at RT. The decompactiontion mix (50 mM DTT, 400 IU/ml heparin, 0.2% Triton in PBS) was added to each dried sperm drop for 2 min and the decompaction was stopped by placing the slides in 4% PFA for 15 min. After washing with PBS for 5 min, the slides were stained with DAPI and mounted using Dako fluorescent mounting medium. Fluorescent images were captured by a Zeiss inverted microscope under a 63X numeric aperture oil-immersion lens (Carl Zeiss). The size of spermatozoa heads was calculated with ImageJ software.

Spermatogenic cell fraction purification

Spermatogenic cell fraction purification was performed as previously described (Shiota et al. 2018).

RNA-seq: WT and *Atad2* KO homozygote male pups were sacrificed by cervical dislocation at 20, 22, 24 and 26 days post-birth and their testes were harvested. RNA was extracted in TRIzol™ reagent, DNA was digested with DNase I and samples were sent for RNA-sequencing.

Alignment. The fastq files were aligned on the UCSC mm10 genome using STAR (2.7.11b) (Dobin et al. 2013) to produce bam files.

Counts. Bam files were counted using HTSeq framework (2.0.5) (Anders et al. 2015), with options: -t exon -f bam -r pos –stranded=reverse -m intersection-strict –nonunique none

Normalization and Differential Analysis. Normalization and differential analysis were performed using the R software [R Core Team. R: A language and environment for statistical computing. Vienna, Austria: R Foundation for Statistical Computing, 2017], (Anders and Huber 2010) DESeq2 (1.22.2) (Anders and Huber 2010; Love et al. 2014) and SARTools (Varet et al. 2016) packages.

Since **d20 WT rep2 sample** has been considered as an outlier, it has been discarded.

QUANTIFICATION AND STATISTICAL ANALYSIS

Statistical analysis was performed with R and GraphPad Prism 8. The results of fertility tests were analyzed by Student t-test. Pairwise Student t-test was used to analyze testis weights and spermatozoa counts of same-aged mice and ratio pairwise Student t-test was used for the IVF efficiency results. The results of sperm decompaction test were analyzed by two-way ANOVA and Tukey's HSD post two-way ANOVA test was used to determine the significance between groups. *P-values* < 0.05 were considered statistically significant: $*p < 0.05$, $**p < 0.01$, $***p < 0.001$.

Data availability

Transcriptomic data presented here were deposited with GEO under the accession N°. GSE277943.

To review GEO accession GSE277943:

Go to https://www.ncbi.nlm.nih.gov/geo/query/acc.cgi?acc=GSE277943

Enter token wrszesqgjfkxxmx into the box

Immunoblot raw data used in preparing the figures are presented as **Supplementary file 1**

Manuscript preparation

The language has been optimized in parts of the text, using free online tools (ChatGPT, Deepl).

COMPETING INTEREST STATEMENT

The authors declare that they have no conflict of interest.

ACKNOWLEDGEMENTS

This work was supported by ANR EpiSperm 4 (ANR-19-CE12- 0014), ANR Episperm 5 (ANR-23-CE12-0028), ANR NME-CoA (ANR-23-CE14-0050) and the Cancer ITMO [Multi-Organisation Thematic Institute of the French Alliance for Life Sciences and Health (AVIESAN)] MIC program to SK and SR. AL is a recipient of a 4th year PhD fellowship by Foundation pour la Recherche Médicale (FRM). High throughput sequencing was performed at the TGML Platform, supported by grants from Inserm, GIS IBiSA, Aix-Marseille Université. We thank Dr. Alexandra Varga for X-gal staining of testis sections.

AUTHOR CONTRIBUTIONS

AL: experimentation, data interpretation, writing and preparation of the manuscript, FB: supervision, experimentation, data interpretation, writing and preparation of the manuscript, management of acquisition of *Atad2* KO mouse model. SB: experimentation and the maintain of *Atad2* mouse model, EL and CA *in vitro* fertilization essays. FC and EBF transcriptomic data analyses. DePu and CG: transcriptomic data generation, SR: founding acquisition and transcriptomic analysis. DaPe and AV experimentation and data generation and analyses. SK: conception, founding acquisition and supervision and coordination of the whole project and writing of the manuscript.

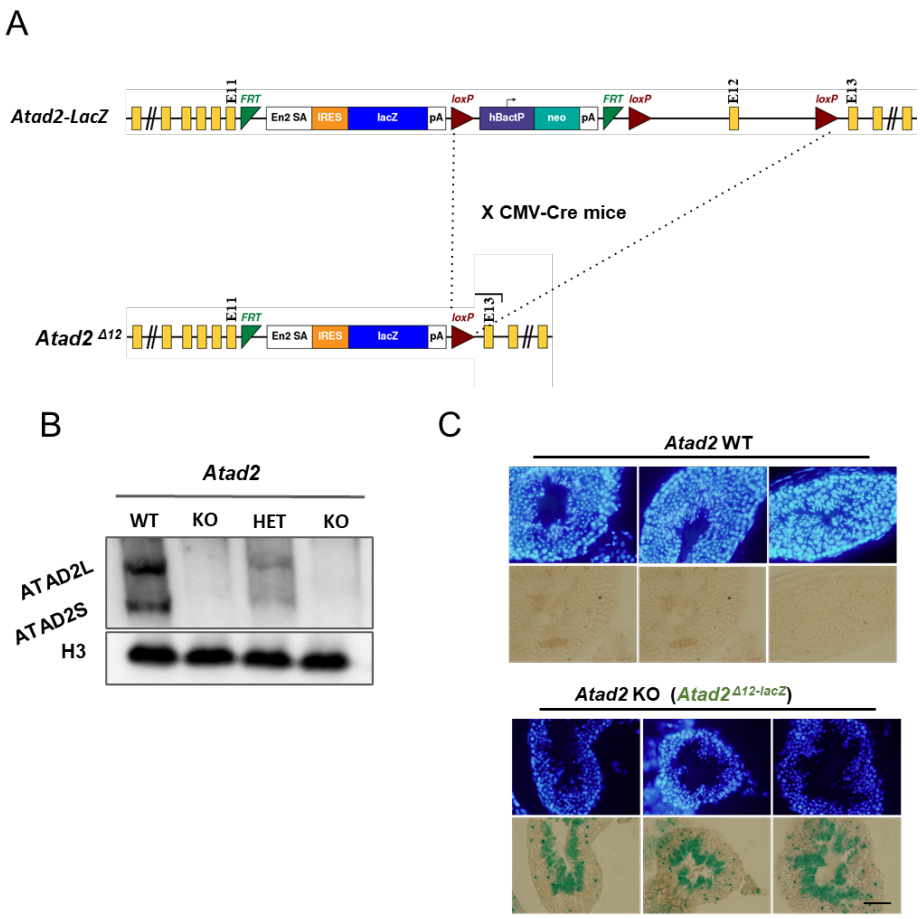

Figure 1: Atad2 is highly expressed in post-meiotic male germ cells.

(**A**) The targeted insertion of the *Lac-Z Lox-Neo-Lox* cassette on the *Atad2* locus on mouse chromosome 15 is represented. The construct contains Cre-recombinase recognition sites (*loxP*) flanking the neo cassette and *Atad2* Exon 12. Crossing mice bearing this construct with *CMV-Cre-recombinase* transgenic mice produced the *Atad2 LacZ*$^{\Delta Neo\text{-}Exon12}$ allele. E = Exon.

(**B**) Extracts from wild-type and *Atad2* KO mice testes were probed with anti-ATAD2 and anti-H3 antibodies as indicated. Four different mice were used for this experiment.

(**C**) Seminiferous tubules sections from wild-type and *Atad2* KO mice were stained with X-gal to visualize *lacZ* gene expression and β -galactosidase activity under the endogenous *Atad2* gene promoter. Testes from three different wild-type and *Atad2* KO mice were used to generate the represented sections. Scale bar: 200 µm

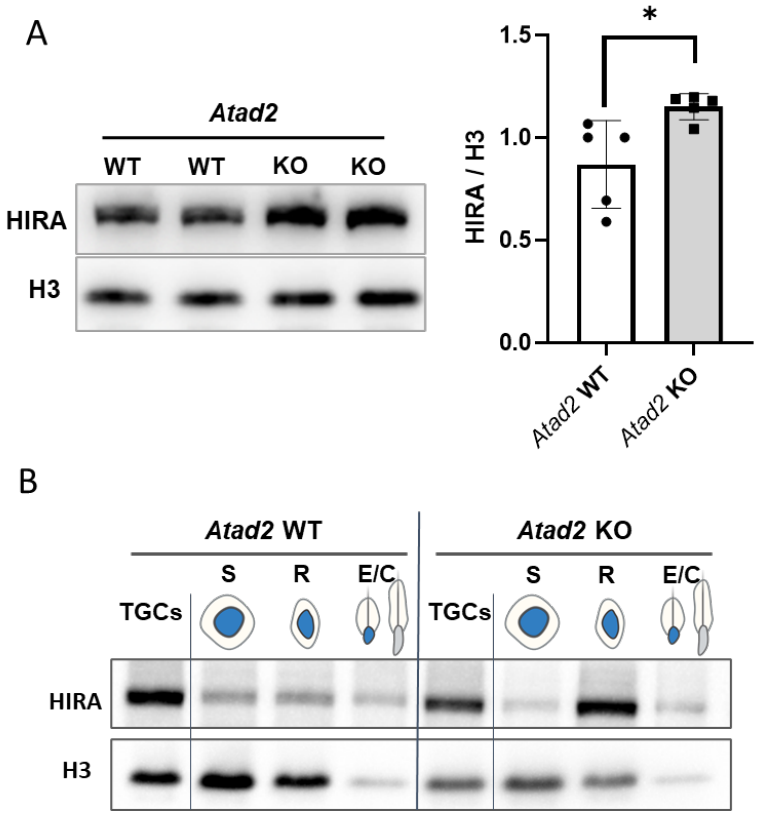

Figure 2: *Atad2* gene inactivation leads to the accumulation of HIRA

(**A**) Total testes' extracts from individual wild-type or Atad2 KO mice (n =5) were used to detect HIRA and H3 by immunoblotting. The panel shows a representative immunoblotting after HIRA detection. The histogram shown in the lower left panel represents quantification of HIRA immunoblotting signal normalized to H3. Mean ± Standard Deviation is 0.8699± 0.2138 and 1.150± 0.06367 for wild type and *Atad2* KO samples respectively and the p value is 0.0228 for unpaired Student t-test.

(**B**) Extracts from fractionated spermatogenic cells (pool of testes from 3 individuals per genotype) were used to detect HIRA and H3.

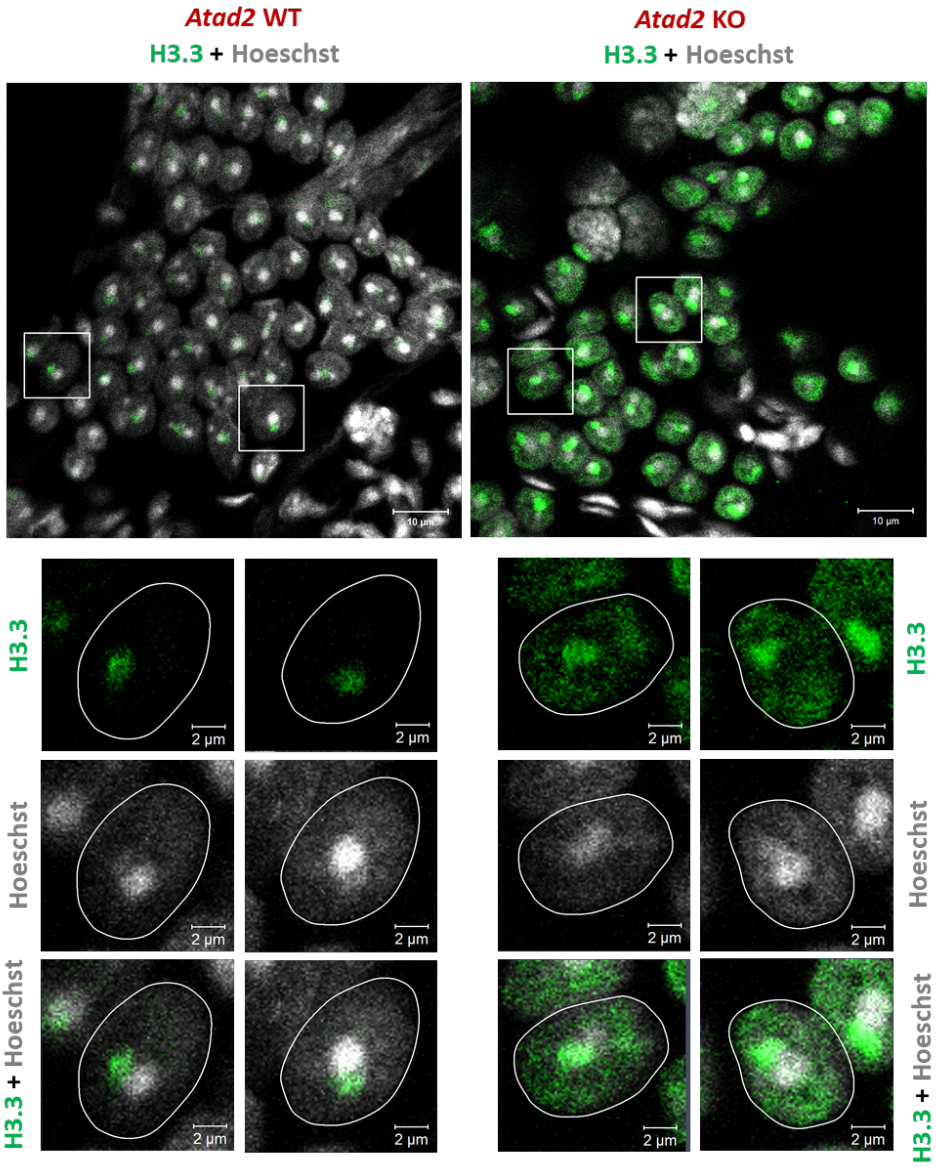

Figure 3: Enhanced H3.3 detection in *Atad2* KO post-meiotic cells

A specific antibody against H3.3 was used to detect H3.3 in round spermatid cells from WT and *Atad2* KO mice. Round spermatids are recognizable thanks to their unique Hoechst - bright chromocenter. The lower panels represent the magnification of selected cells shown at a lower magnification in the upper panels. The images show H3.3 labelling and Hoechst staining alone or the merged images of these staining as indicated.

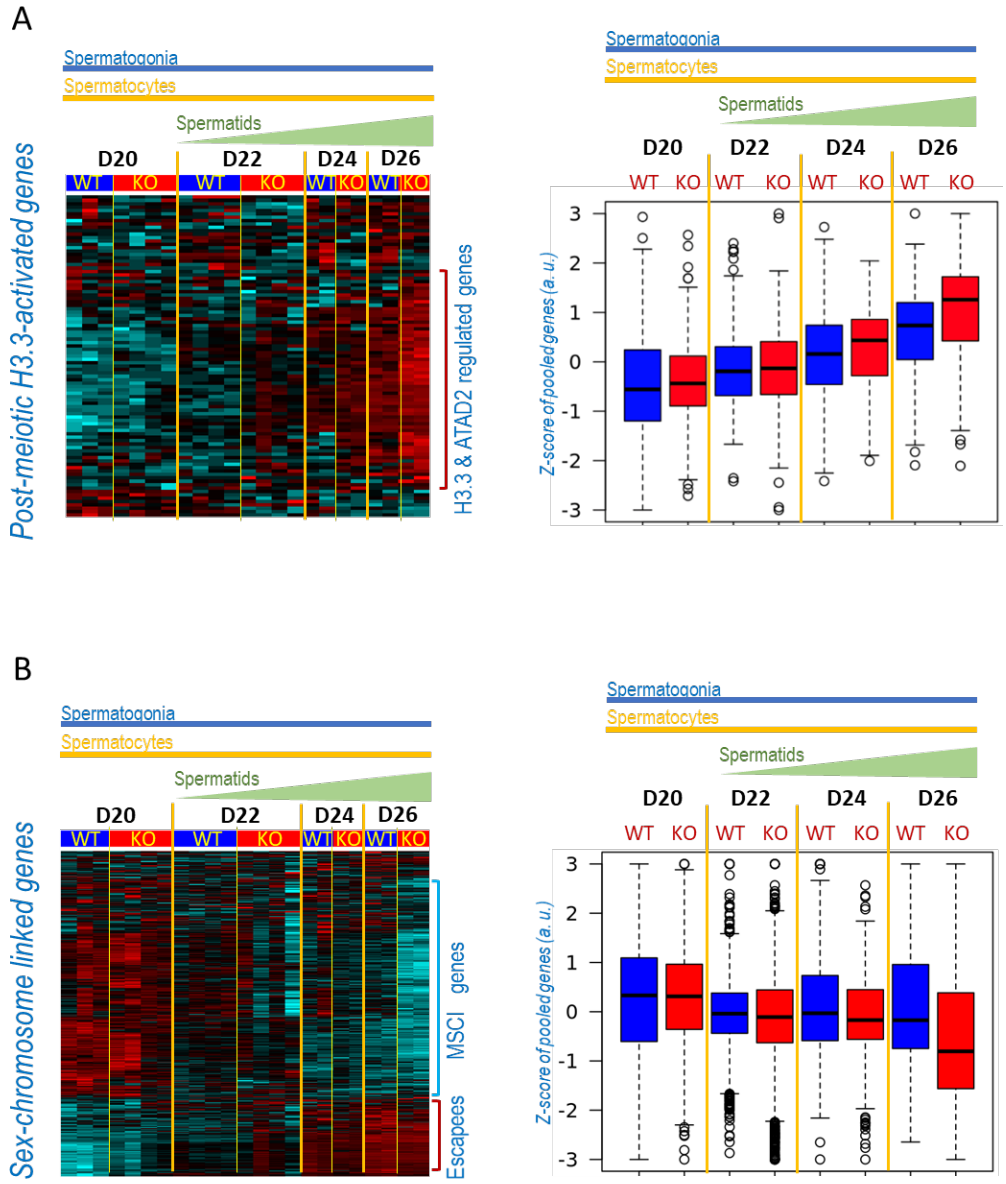

Figure 4: ATAD2 enhances H3.3 gene regulatory functions

(**A**) Mouse testes harvested at the indicated post-partum days (day 20 (D20, 3 samples for WT and 4 samples for *Atad2* KO), day 22 (4 samples for WT and 4 samples for *Atad2* KO), day 24 (2 samples for WT and 2 samples for *Atad2* KO) and day 26 (2 samples for WT and 2 samples for *Atad2* KO)), were used to extract total RNAs which were then sequenced. The published list of genes that were found to be down-regulated in the absence of H3.3 (Fontaine et al. 2022) were used to monitor their expression as a function of the appearance of specific cell types as indicated in the diagram above the heatmaps. Down regulated genes of SUP_TABLE_2.xlsx tables (Fontaine et al. 2022) were obtained by filtering genes according to

log2(KO/WT) column less than 0. Samples corresponding to wild-type (WT) and *Atad2* KO (KO) mice are shown. Expression of each gene is normalized (z-score). Boxplots in the right panel show the standardized expression of grouped genes presented individually on the heatmap, as a function of PP days, as indicated. The black bar in each boxplot correspond to the mean expression value. Data from Atad2 WT samples are in blue and data from Atad2 KO samples are in red.

(**B**) The analyses described in (A) were performed but this time the expression of genes present on the sex chromosomes were considered. MSCI: Meiotic sex chromosome inactivation. Escapees: genes that escape MSCI in post-meiotic cells.

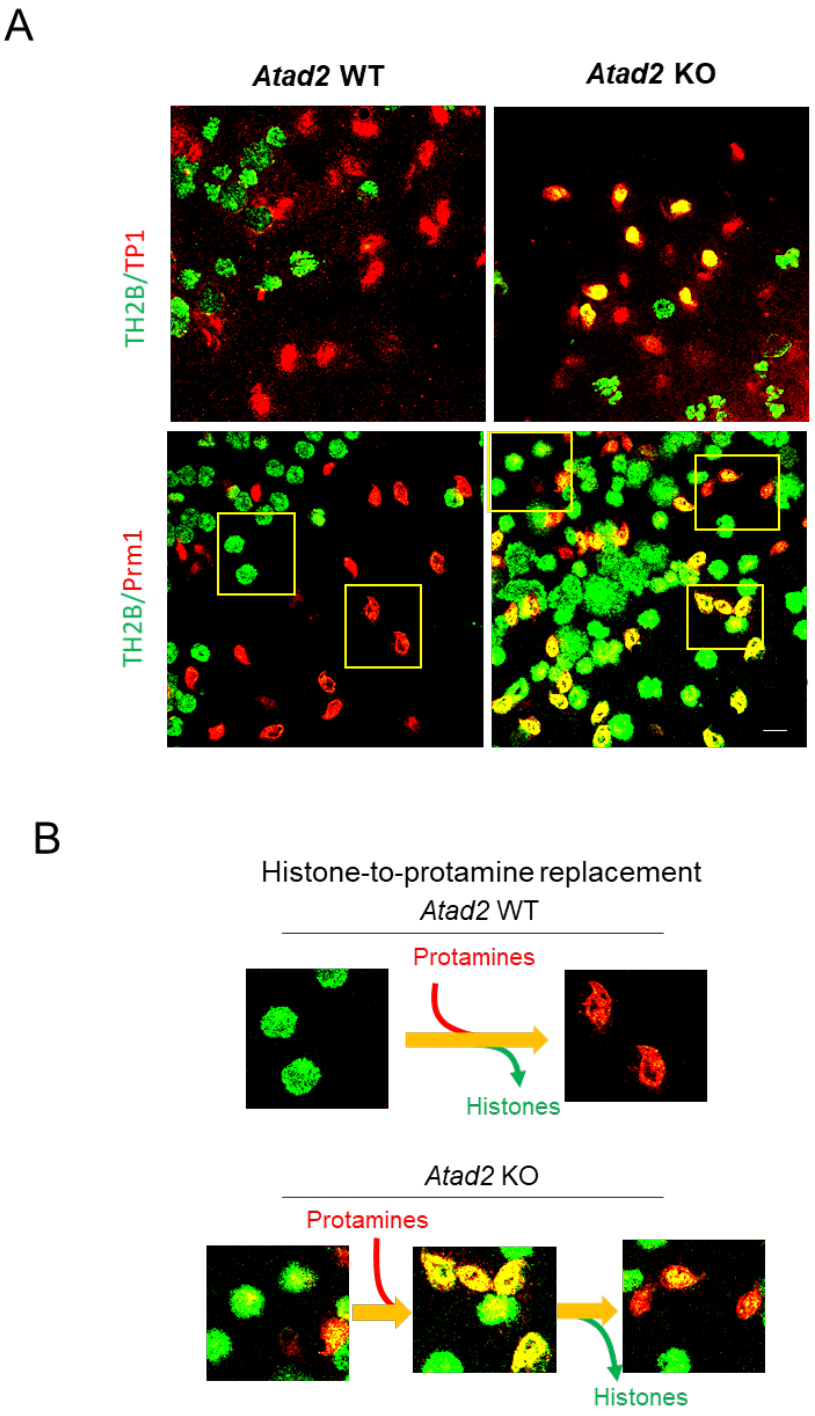

Figure 5: Atad2 is required for efficient histone-to-protamine replacement.

(**A**) Spermatogenic cell preparations from wild-type and *Atad2* KO mice were stained with antibodies against TH2B (in green) and transition protein 1 (TP1) or protamine 1 (Prm1) (in

red). A yellow signal indicates the co-detection of TH2B along with TP1 or Prm1. The indicated fields are shown at higher magnification in panel “B”. Scale bar: 10 µm.

(**B**) Fields shown in panel “A” are ordered to illustrate the transition from the histone associated genome to its packaging by protamines, considering both wild-type and *Atad2* KO spermatogenic cells.

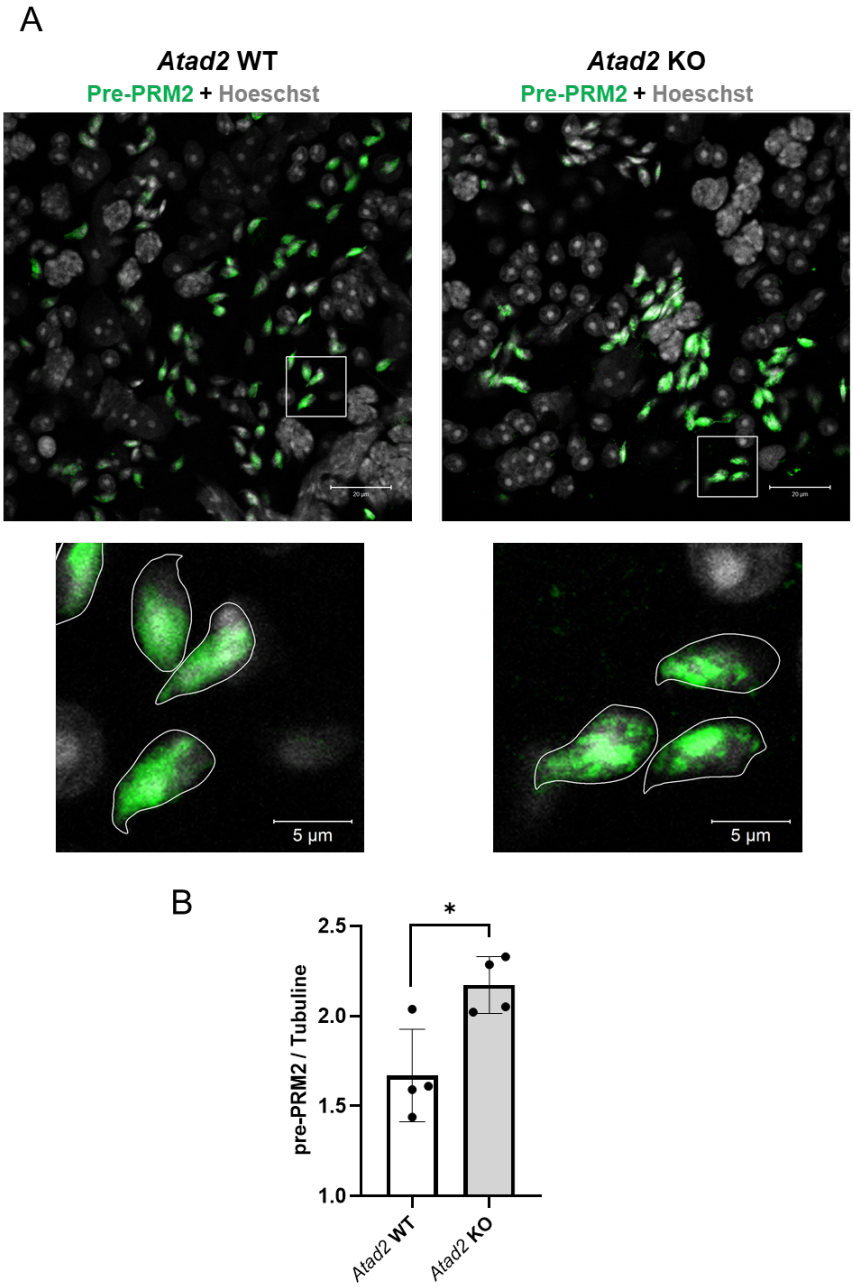

Figure 6: Atad2 is required for proper pre-protamine 2 processing and protamine assembly

(**A**) A specific antibody raised against the processed part of pre-PRM2 (Rezaei-Gazik et al. 2022) was used to detect pre-PRM2 expression and localization in tubular elongating spermatid cells. The lower panels represent the magnification of selected cells.

(**B**) The amount of pre-PRM2 was detected using soluble extracts from testis of wild-type and *Atad2* KO mice using ELISA. Histograms show the normalized values (pre-PRM2/tubulin) of 4 measurements of sedimentation samples of Elongating/Condensing fractions. Mean ±

Standard Deviation is 1.670 ± 0.2572 and 2.172 ± 0.1576 for wild type and *Atad2* KO samples respectively and the p value equals 0.0158 when applying unpaired *Student t-test*.

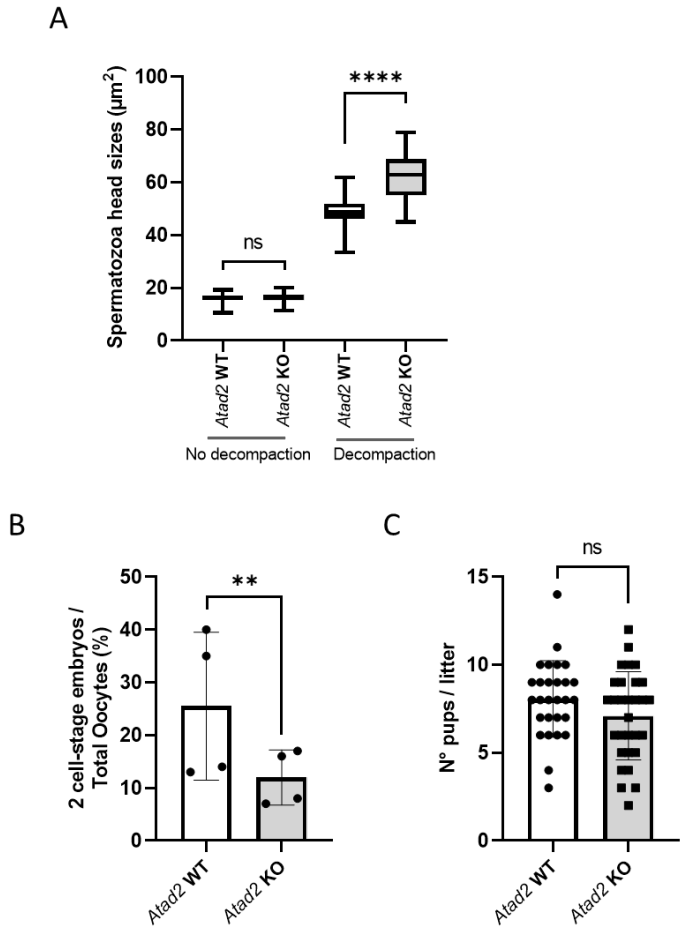

Figure 7: ATAD2s' function in sperm genome compaction and fertility parameters

(**A**) Epididymal sperm cells were isolated by the swim-up method from wild-type or *Atad2* KO mice and underwent a decompaction test and the sizes of the sperm heads were measured and represented as box plots (*n* = 75 sperm heads / box plot). The value ranges (mean) were 10.4 ~ 19.3 (16.0) for wild type sperms without decompaction; 11.4 ~ 20.1 (16.4) for *Atad2* KO sperms without decompaction; 33.4 ~ 61.8 (48.5) for wild type sperms after decompaction; 45.0 ~ 78.9 (62.6) *Atad2* KO sperms after decompaction. Tukey's HSD post two-way ANOVA test was used. ****$p < 0.001$.

(**B**) Pools of ocytes from C57BL6 females were obtained and used for *in vitro* fertilization (IVF) with spermatozoa from WT or *Atad2* KO males (the experiment was repeated 4 times independently). The fertilization success rate is indicated as a percentage of oocytes giving rise to stage 2 embryos. Mean ± Standard Deviation is 25.50 ± 14.01 and 12.00 ± 5.228 for

wild type and *Atad2* KO experiments respectively and the p = 0.0020 for ratio paired *Student t-test*.

(**C**) Wild-type (*n* = 5) and *Atad2* KO (*n* = 5) male mice were crossed with C57BL6 female mice and the number of pups was counted and reported as box plots (*n* = 28 and 30, respectively). The average numbers of pups are respectively 8.071 ± 2.176 and 7.100 ± 2.510 and the *p-value of Student t-test* = 0.1221.

REFERENCES

Anders S, Huber W. 2010. Differential expression analysis for sequence count data. *Genome Biol* **11**: R106.

Anders S, Pyl PT, Huber W. 2015. HTSeq--a Python framework to work with high-throughput sequencing data. *Bioinformatics* **31**: 166-169.

Bao J, Bedford MT. 2016. Epigenetic regulation of the histone-to-protamine transition during spermiogenesis. *Reproduction* **151**: R55-70.

Barral S, Morozumi Y, Hoghoughi N, Rousseaux S, Khochbin S. 2017a. [The mystery of histone disappearance during spermatogenesis]. *Med Sci (Paris)* **33**: 588-590.

Barral S, Morozumi Y, Tanaka H, Montellier E, Govin J, de Dieuleveult M, Charbonnier G, Coute Y, Puthier D, Buchou T et al. 2017b. Histone Variant H2A.L.2 Guides Transition Protein-Dependent Protamine Assembly in Male Germ Cells. *Mol Cell* **66**: 89-101 e108.

Bashiri Z, Amidi F, Amiri I, Zandieh Z, Maki CB, Mohammadi F, Amiri S, Koruji M. 2021. Male Factors: the Role of Sperm in Preimplantation Embryo Quality. *Reprod Sci* **28**: 1788-1811.

Boussouar F, Jamshidikia M, Morozumi Y, Rousseaux S, Khochbin S. 2013. Malignant genome reprogramming by ATAD2. *Biochim Biophys Acta* **1829**: 1010-1014.

Caron C, Lestrat C, Marsal S, Escoffier E, Curtet S, Virolle V, Barbry P, Debernardi A, Brambilla C, Brambilla E et al. 2010. Functional characterization of ATAD2 as a new cancer/testis factor and a predictor of poor prognosis in breast and lung cancers. *Oncogene* **29**: 5171-5181.

Cattaneo M, Morozumi Y, Perazza D, Boussouar F, Jamshidikia M, Rousseaux S, Verdel A, Khochbin S. 2014. Lessons from yeast on emerging roles of the ATAD2 protein family in gene regulation and genome organization. *Mol Cells* **37**: 851-856.

Dobin A, Davis CA, Schlesinger F, Drenkow J, Zaleski C, Jha S, Batut P, Chaisson M, Gingeras TR. 2013. STAR: ultrafast universal RNA-seq aligner. *Bioinformatics* **29**: 15-21.

Fontaine E, Papin C, Martinez G, Le Gras S, Nahed RA, Hery P, Buchou T, Ouararhni K, Favier B, Gautier T et al. 2022. Dual role of histone variant H3.3B in spermatogenesis: positive regulation of piRNA transcription and implication in X-chromosome inactivation. *Nucleic Acids Res* **50**: 7350-7366.

Gaucher J, Reynoird N, Montellier E, Boussouar F, Rousseaux S, Khochbin S. 2010. From meiosis to postmeiotic events: the secrets of histone disappearance. *FEBS J* **277**: 599-604.

Gaucher JF, Mauge C, Didry D, Guichard B, Renault L, Carlier MF. 2012. Interactions of isolated C-terminal fragments of neural Wiskott-Aldrich syndrome protein (N-WASP) with actin and Arp2/3 complex. *J Biol Chem* **287**: 34646-34659.

Goudarzi A, Zhang D, Huang H, Barral S, Kwon OK, Qi S, Tang Z, Buchou T, Vitte AL, He T et al. 2016. Dynamic Competing Histone H4 K5K8 Acetylation and Butyrylation Are Hallmarks of Highly Active Gene Promoters. *Mol Cell* **62**: 169-180.

Hammond CM, Bao H, Hendriks IA, Carraro M, Garcia-Nieto A, Liu Y, Reveron-Gomez N, Spanos C, Chen L, Rappsilber J et al. 2021. DNAJC9 integrates heat shock molecular chaperones into the histone chaperone network. *Mol Cell* **81**: 2533-2548 e2539.

Hoghoughi N, Barral S, Vargas A, Rousseaux S, Khochbin S. 2018. Histone variants: essential actors in male genome programming. *J Biochem* **163**: 97-103.

Jang J, Kang Y, Zofall M, Cho C, Grewal S, Lee JY. 2024. Abo1 ATPase facilitates the dissociation of FACT from chromatin. *bioRxiv*.

Krastev DB, Li S, Sun Y, Wicks AJ, Hoslett G, Weekes D, Badder LM, Knight EG, Marlow R, Pardo MC et al. 2022. The ubiquitin-dependent ATPase p97 removes cytotoxic trapped PARP1 from chromatin. *Nat Cell Biol* **24**: 62-73.

Lafon A, Taranum S, Pietrocola F, Dingli F, Loew D, Brahma S, Bartholomew B, Papamichos-Chronakis M. 2015. INO80 Chromatin Remodeler Facilitates Release of RNA Polymerase II from Chromatin for Ubiquitin-Mediated Proteasomal Degradation. *Mol Cell* **60**: 784-796.

Le Blevec E, Muronova J, Ray PF, Arnoult C. 2020. Paternal epigenetics: Mammalian sperm provide much more than DNA at fertilization. *Mol Cell Endocrinol* **518**: 110964.

Lin CJ, Koh FM, Wong P, Conti M, Ramalho-Santos M. 2014. Hira-mediated H3.3 incorporation is required for DNA replication and ribosomal RNA transcription in the mouse zygote. *Dev Cell* **30**: 268-279.

Liu H, Wen Q, Yan S, Zeng W, Zou Y, Liu Q, Zhang G, Zou J, Zou X. 2022. Tumor-Promoting ATAD2 and Its Preclinical Challenges. *Biomolecules* **12**.

Love MI, Huber W, Anders S. 2014. Moderated estimation of fold change and dispersion for RNA-seq data with DESeq2. *Genome Biol* **15**: 550.

Montellier E, Boussouar F, Rousseaux S, Zhang K, Buchou T, Fenaille F, Shiota H, Debernardi A, Hery P, Curtet S et al. 2013. Chromatin-to-nucleoprotamine transition is controlled by the histone H2B variant TH2B. *Genes Dev* **27**: 1680-1692.

Moriniere J, Rousseaux S, Steuerwald U, Soler-Lopez M, Curtet S, Vitte AL, Govin J, Gaucher J, Sadoul K, Hart DJ et al. 2009. Cooperative binding of two acetylation marks on a histone tail by a single bromodomain. *Nature* **461**: 664-668.

Morozumi Y, Boussouar F, Tan M, Chaikuad A, Jamshidikia M, Colak G, He H, Nie L, Petosa C, de Dieuleveult M et al. 2016. Atad2 is a generalist facilitator of chromatin dynamics in embryonic stem cells. *J Mol Cell Biol* **8**: 349-362.

Nashun B, Hill PW, Smallwood SA, Dharmalingam G, Amouroux R, Clark SJ, Sharma V, Ndjetehe E, Pelczar P, Festenstein RJ et al. 2015. Continuous Histone Replacement by Hira Is Essential for Normal Transcriptional Regulation and De Novo DNA Methylation during Mouse Oogenesis. *Mol Cell* **60**: 611-625.

Okada Y. 2022. Sperm chromatin condensation: epigenetic mechanisms to compact the genome and spatiotemporal regulation from inside and outside the nucleus. *Genes Genet Syst* **97**: 41-53.

Puumalainen MR, Lessel D, Ruthemann P, Kaczmarek N, Bachmann K, Ramadan K, Naegeli H. 2014. Chromatin retention of DNA damage sensors DDB2 and XPC through loss of p97 segregase causes genotoxicity. *Nat Commun* **5**: 3695.

Rezaei-Gazik M, Vargas A, Amiri-Yekta A, Vitte AL, Akbari A, Barral S, Esmaeili V, Chuffart F, Sadighi-Gilani MA, Coute Y et al. 2022. Direct visualization of pre-protamine 2 detects protamine assembly failures and predicts ICSI success. *Mol Hum Reprod* **28**.

Rousseaux S, Reynoird N, Khochbin S. 2022. NUT Is a Driver of p300-Mediated Histone Hyperacetylation: From Spermatogenesis to Cancer. *Cancers (Basel)* **14**.

Shiota H, Barral S, Buchou T, Tan M, Coute Y, Charbonnier G, Reynoird N, Boussouar F, Gerard M, Zhu M et al. 2018. Nut Directs p300-Dependent, Genome-Wide H4 Hyperacetylation in Male Germ Cells. *Cell Rep* **24**: 3477-3487 e3476.

Skarnes WC, Rosen B, West AP, Koutsourakis M, Bushell W, Iyer V, Mujica AO, Thomas M, Harrow J, Cox T et al. 2011. A conditional knockout resource for the genome-wide study of mouse gene function. *Nature* **474**: 337-342.

Tang MC, Jacobs SA, Mattiske DM, Soh YM, Graham AN, Tran A, Lim SL, Hudson DF, Kalitsis P, O'Bryan MK et al. 2015. Contribution of the two genes encoding histone variant h3.3 to viability and fertility in mice. *PLoS Genet* **11**: e1004964.

van den Berg SJW, East S, Mitra S, Jansen LET. 2023. p97/VCP drives turnover of SUMOylated centromeric CCAN proteins and CENP-A. *Mol Biol Cell* **34**: br6.

van den Boom J, Wolf M, Weimann L, Schulze N, Li F, Kaschani F, Riemer A, Zierhut C, Kaiser M, Iliakis G et al. 2016. VCP/p97 Extracts Sterically Trapped Ku70/80 Rings from DNA in Double-Strand Break Repair. *Mol Cell* **64**: 189-198.

van der Heijden GW, Derijck AA, Posfai E, Giele M, Pelczar P, Ramos L, Wansink DG, van der Vlag J, Peters AH, de Boer P. 2007. Chromosome-wide nucleosome replacement and H3.3 incorporation during mammalian meiotic sex chromosome inactivation. *Nat Genet* **39**: 251-258.

Varet H, Brillet-Gueguen L, Coppee JY, Dillies MA. 2016. SARTools: A DESeq2- and EdgeR-Based R Pipeline for Comprehensive Differential Analysis of RNA-Seq Data. *PLoS One* **11**: e0157022.

Wang T, Perazza D, Boussouar F, Cattaneo M, Bougdour A, Chuffart F, Barral S, Vargas A, Liakopoulou A, Puthier D et al. 2021. ATAD2 controls chromatin-bound HIRA turnover. *Life Sci Alliance* **4**.

Yuen BT, Bush KM, Barrilleaux BL, Cotterman R, Knoepfler PS. 2014. Histone H3.3 regulates dynamic chromatin states during spermatogenesis. *Development* **141**: 3483-3494.

Supplementary materials

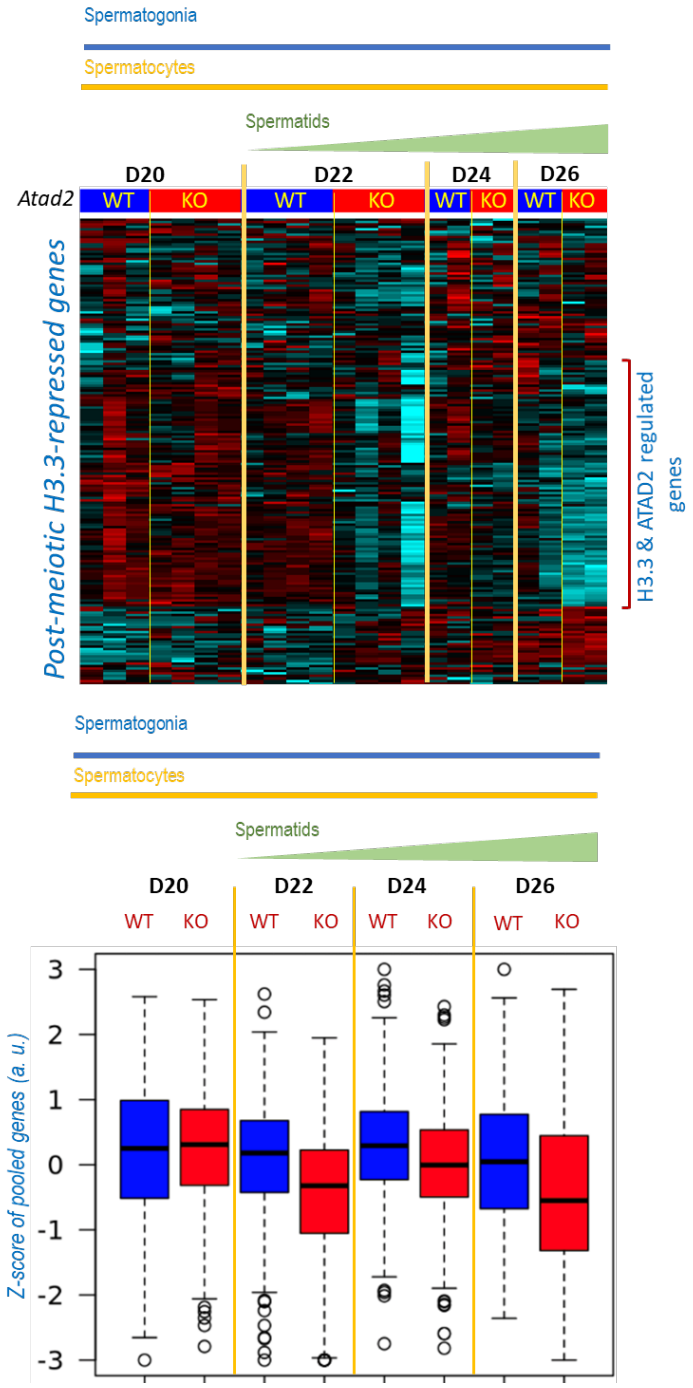

Figure S1: ATAD2 enhances H3.3 gene regulatory functions

The same analyses as described in the legend of Figure 4 were performed except that the published list of genes that are normally repressed by H3.3 (activated in the absence of H3.3) in post-meiotic cells (from Fontaine et al. 2022) is considered.

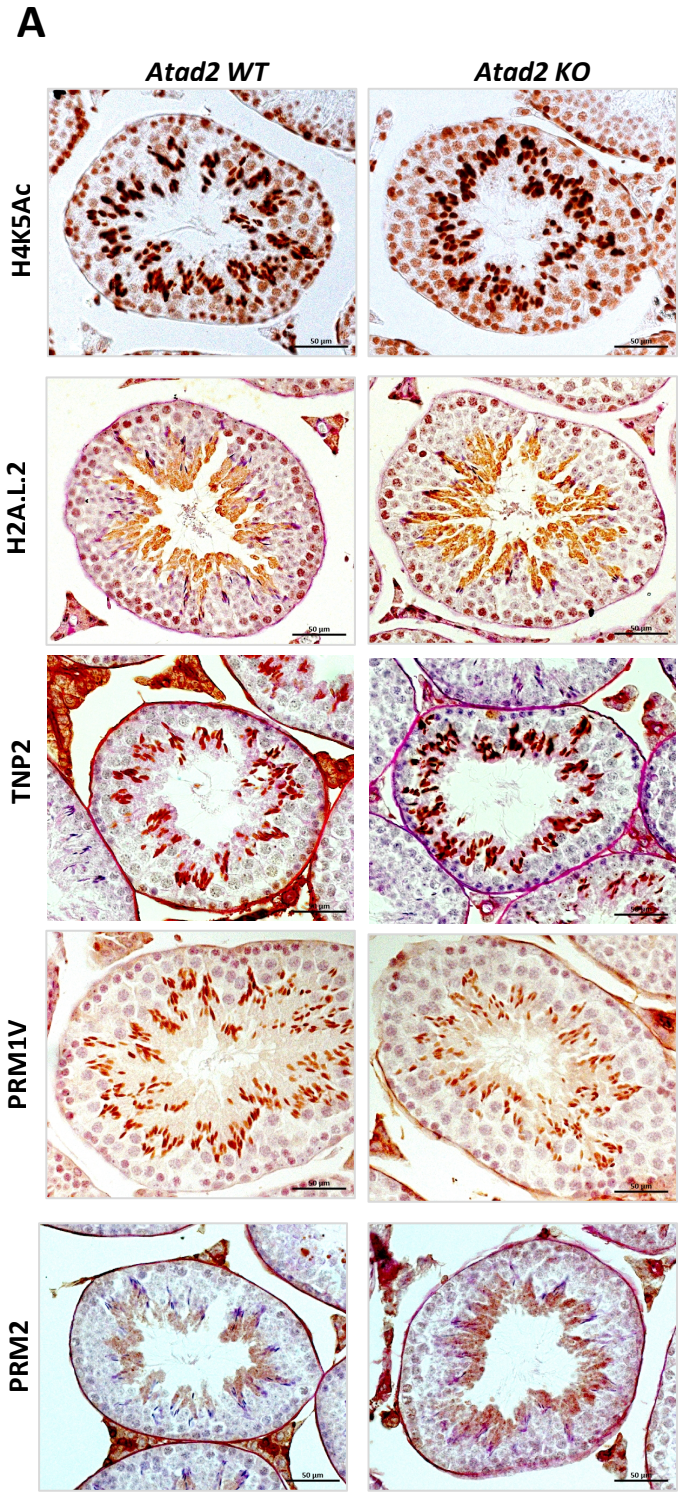

Figure S2: *Atad2* gene inactivation does not significantly disturb the testis histology as well as occurrence of H4K5ac, and the accumulation of H2A.L.2, TP2, PRM1 and PRM2 cell type-specific accumulation. Sections of paraffin-embedded testes from wild-type or *Atad2* KO mice were used to visualize the accumulation H4K5ac or expression of H2A.L.2, TP2, PRM1 and PRM2.

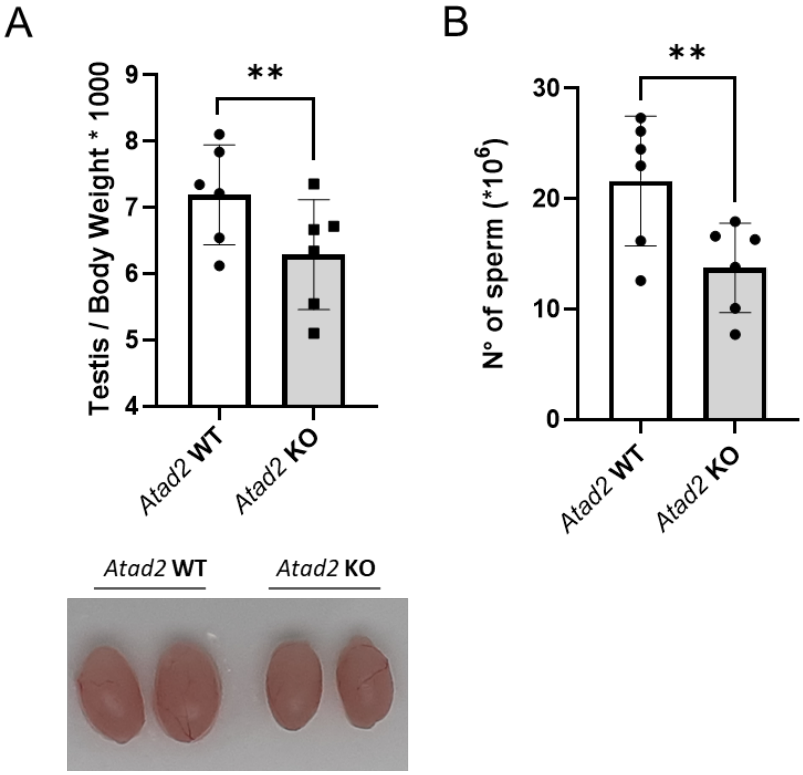

Figure S3: *Atad2* depletion affects testis weight and mature sperm counts.
(**A**)Testes (n = 6) from 21-27 weeks old wild-type and *Atad2* KO mice were weighted and normalized to body weight and only same-age mice were compared pairwise. Histograms represent the mean of the measured weights and error bars the Standard Deviation. The *p*-value of pairwise *Student t-test* = 0.0041 (upper panel). The lower panel shows representative testes from wild-type and *Atad2* KO mice.
(B) Spermatozoa counts (Cells /ml) were performed for pairs of wild type and *Atad2* KO (*n=6*). The average numbers of spermatozoa counts are respectively 21.61 ± 5.884 and 13.74 ± 4.055 and the *p*-value of *paired Student t-test* = 0.0010.

Table S1: Primary Antibodies

Name	Company	Reference	Host Species	Dilution
Anti-ATAD2	Homemade	-	Rabbit	1:1000
anti-H2A.L1/L2 SAB771	Homemade	-	Rabbit	1:200 for IHC
Anti-Histone H3 antibody - Nuclear Marker and ChIP Grade	Abcam	Ab1791	Rabbit	1:5000 for WB
Anti-H2B (testis specific)	Abcam	AB178426	Rabbit	1:100 for IF
anti-H3F3B	Abnova	#H00003021-M01	Mouse	1:200 for IF
Anti-H4K5Ac	PTM Biolabs	#PTM-163	Mouse	1:200 for IHC
Anti-HIRA	Cell Signaling Technology	D6O8L	Rabbit	1:1000 for WB
Pre-PRM2	Homemade	-	Rabbit	1:100 for IF
anti-Protamine 1	BRIAR Patch Biosciences	HUP1N	Mouse	1:200 for IHC/IF
anti-Protamine 2	BRIAR Patch Biosciences	HUP2B	Mouse	1:200 for IHC
Anti-TNP2 (B-2)	Santa Cruz Biotechnology	sc-393843	Mouse	1:200 for IHC
Goat anti Rabbit IgG (H + L)-HRP	Bio-rad	Cat# 1706515	-	1:5000 for WB
Goat anti-Mouse IgG (H + L)-HRP	Bio-rad	Cat# 1706516	-	1:5000 for WB
Alexa Fluor™ 568 goat Anti-mouse IgG (H+L)	Invitrogen	Cat# A11004	-	1:500 for IF
Alexa Fluor™ 488 goat Anti-rabbit IgG (H+L)	Invitrogen	Cat# A11034	-	1:500 for IF

WB: Western Blot Analysis, IF: Immunofluorescence and IHC: Immunohistochemistry.

Table S2: Reagents / Products used

Products	Company	Reference
Bovine Serum Albumine (BSA)	Euromedex	# 04-100-812-C
Clarity™ Western ECL Substrate	Bio-Rad	Cat # 170-5061
Clarity Max™ Western ECL Substrate	Bio-Rad	Cat # 170-5062
Complete Protease inhibitor EDTA-free	Sigma-Aldrich	# 4693159001
Dako Fluorescent Mounting Medium	Dako	S3023
DL-Dithiothreitol (DTT)	Euromedex	EU0006
DNase I recombinant	Roche	4536282001
DPBS	Gibco	14200-075
Ethylenediaminetetraacetic acid disodium salt dihydrate (EDTA)	Sigma-Aldrich	E6635
Ethylene glycol-bis (2-aminoethylether)-N,N,N',N'-tetraacetic acid (EGTA)	Sigma-Aldrich	E3889
Formalin solution, neutral buffered, 10%	Sigma-Aldrich	HT5012
Glutaraldehyde solution	Sigma-Aldrich	G5882
Heparin sodium salt from porcine intestinal mucosa	Sigma-Aldrich	H3149
Hoechst	Invitrogen	# 33342
Human Chorionic Gonadotropin (HCG)	MED-VET	Chorulon 1500 UI
Laemmli Sample Buffer 4x	BioRad	# 1610747
Magnesium Chloride (MgCl2)	Euromedex	2189
Mayer's Hematoxylin Solution	Sigma-Aldrich	MHS16
M2 medium	Sigma-Aldrich	M7167
M16 medium	Sigma-Aldrich	M7292
Nitrocellulose Blotting membrane	Amersham™ Protran®	10600015
Nonidet™ P 40 Substitute (NP 40)	Sigma-Aldrich	74385
NuPAGE™ 4-12% Bis-Tris Gel	Invitrogen	NP0335BOX

Potassium Ferricyanide	Sigma-Aldrich	P-8131
Potassium Ferrocyanide	Sigma-Aldrich	P-9387
Pregnant Mare Serum Gonadotropin (PMSG)	MED-VET	Syncro-part PMSG 600 UI
Saccharose	Sigma-Aldrich	S7903
Saponin from quillaja bark	Sigma-Aldrich	S7900
Sodium deoxycholate (NaDoc)	Sigma-Aldrich	D6750
Superfrost®slides	Thermo Scientific™	LCSF05
TMB ELISA Substrate (High Sensitivity)	Abcam	AB171523
Trans-Blot Turbo 5X Transfer Buffer	BioRad	Cat # 10026938
Triton™ X-100	Sigma-Aldrich	T9284
TRIzol™	Thermo Scientific™	# 15596026
TWEEN® 20	Sigma-Aldrich	P7949
Urea	Sigma-Aldrich	U5378
X-Gal	Invitrogen	B1690
96 Well Round (U) Bottom Plate	Thermo Scientific™	# 163320
450 nm Stop Solution for TMB Substrate	Abcam	AB171529